



# Variability in reconstructed soil bulk density of a high moisture content soil: a study on feature identification and ground penetrating radar detection

Xu Hanxiao<sup>1</sup> · Cao Yingui<sup>1,2</sup> · Luo Gubai<sup>1</sup> · Wang Shufei<sup>1</sup> · Wang Jinman<sup>1,2</sup> · Bai Zhongke<sup>1,2</sup>

Received: 31 March 2021 / Accepted: 22 March 2022 / Published online: 18 April 2022  
© The Author(s), under exclusive licence to Springer-Verlag GmbH Germany, part of Springer Nature 2022

## Abstract

The complex formation process of reconstructed soil triggers the high spatial variability of soil physical properties, for which traditional soil sampling methods are not applicable due to the destructive and time-consuming modes. Ground penetrating radar (GPR) can collect continuous and high-resolution data flexibly, but the technology has rarely been employed to detect reconstructed soil properties in opencast coalmine regions. This study explored the applicability and accuracy of GPR in measuring reconstructed soil bulk density (RSBD) in southern dump, expanded western dump, and internal dump of the Antaibao open-pit mine, China. The variations of RSBD and the relationships between the dielectric constant and RSBD were analyzed based on ring knife sampling weighing, GPR detection, variance analysis, and fitting analysis. The results showed that (1) RSBD exhibited significant variations in different dumps and at different depths of the same profile. (2) RSBD differences in different dumps could be qualitatively analyzed based on the large-amplitude signals in GPR images. (3) When the soil volume moisture content ranged from 15 to 25%, RSBD was found to be negatively correlated with the dielectric constant. GPR has the potential to be widely employed to detect RSBD in reclaimed lands, which can contribute to the development of non-destructive quality testing of land reclamation.

**Keywords** Soil reconstruction · GPR · RSBD · Dielectric constant · Land reclamation

## Introduction

As one of the most important energy sources globally, coal is mostly exploited through open-pit mining (Wang and Zhang 2013). Although the exploited coal supported the development of economics, large-scale coal mining has inevitably triggered severe ecological issues in mining regions (Bunker 1996; Buttel 2002; Wu et al. 2014; Pan et al. 2017; Cao et al. 2017, 2018). For instance, coal mining would produce large amounts of rock fragments and cause serious damage to the ecosystem of mining regions (Wang and Wu 2010; Chen et al. 2016; Berton et al. 2019). Dumps are of high ecological risks, where the ecosystems can be easily destroyed

by the environmental and geological disasters (Andrea 2010; Sun et al. 2015). Therefore, effective land reclamation measures should be adopted to maintain the sustainable development of mining areas (Bian 2005; Kitula 2006; Mondal et al. 2016). During the land reclamation projects in mining areas, the soil physicochemical properties have a substantial impact on the restoration of damaged ecosystems in mining areas (Cao et al. 2015; Anchuela et al. 2016; Han et al. 2016; Ma et al. 2006). As one of the most important soil physical properties, soil bulk density is normally employed to reflect soil compactness and fertility, making it an indispensable indicator for the study of soil moisture and fertilizer conservation (Abu-Hamdeh 2003; Osunbitan et al. 2005; Brahim et al. 2012). In the process of mine dump reclamation, mechanical rolling can easily increase the soil bulk density (Cao et al. 2013; Li et al. 2001, 2002), which further adversely affects vegetation growth and hinders the restoration of the damaged ecosystem in mining areas.

It is complicated to reconstruct reclaimed soil physicochemical properties due to their high spatial heterogeneity. Traditional soil sampling methods are not suitable for

✉ Cao Yingui  
caoyingui1982@126.com

<sup>1</sup> School of Land Science and Technology, China University of Geosciences, Beijing 100083, China

<sup>2</sup> Key Laboratory of Consolidation and Rehabilitation Ministry of Natural Resources, Beijing 100035, China

the large-scale spatial investigation of soil differentiation and formation mechanisms due to the limitations of geological background, high cost of manpower, and resources (Olhoeft 2000; Jonard et al. 2013; Luo et al. 2019a, b). Compared with other detection methods, it has the advantages of a non-destructive technology used for the detection of underground targets, GPR is mainly characterized by fast detection speed, continuous detection process, high resolution, and flexible operation (Wang et al. 2016a, b). Research has been carried out locally and abroad, on the detection of soil physical properties through GPR, but there are fewer studies on reconstructed soil bulk density (RSBD) in reclaimed areas. Most studies were only established on laboratory experiments that explored the theoretical aspects of non-destructive GPR detection (Wang et al. 2016a, b). Previous studies showed that the dielectric constant is positively correlated with soil bulk density when the moisture content is less than 0.5% (Plati and Loizos 2013). However, volumetric moisture contents are normally higher than 0.5% under natural conditions, for which more theoretical evidence should be explored to support the application of GPR in detecting soil bulk density. Additionally, there are few studies on the correlation between soil bulk density and dielectric constants; the correlation between soil bulk density and dielectric constants is rarely investigated under other soil bulk moisture contents (Luo et al. 2019a, b), which has hindered the potential application and popularization of this technology

in reconstructing soil physical properties in mining reclamation projects.

Therefore, this study mainly aims to: (1) explore the variations of RSBD in the southern dump, expanded western dump, and internal dump of the Antaibao open-pit mine in Pingshuo, China; (2) analyze the relationship between the dielectric constant and RSBD based on ring knife sampling weighing, GPR detection, variance analysis, and fitting analysis; (3) verify the feasibility of GPR in detecting RSBD and provide some insight into the rapid and non-destructive detection of RSBD in reclaimed lands.

## Materials and methods

### Research area overview

The study area is located in the Antaibao open-pit mine that is the border among Shanxi, Inner Mongolia, and Shanxi (Fig. 1). In this zone, the estimated coal reserve is approximately 12.70 billion tons. The Antaibao open-pit mine is located within  $112^{\circ} 11' - 113^{\circ} 30' E$  and  $39^{\circ} 23' - 39^{\circ} 37' N$ . It has a temperate semiarid continental climate with strong winds in winter and spring. Annually, the wind speed exceeds  $8 \text{ m s}^{-1}$  for more than 35 days (sometimes reaching 45 days), resulting in strong soil physical weathering. The annual average temperature is  $4.8 - 7.8^{\circ} C$ , and the annual precipitation is approximately 450 mm and is mainly

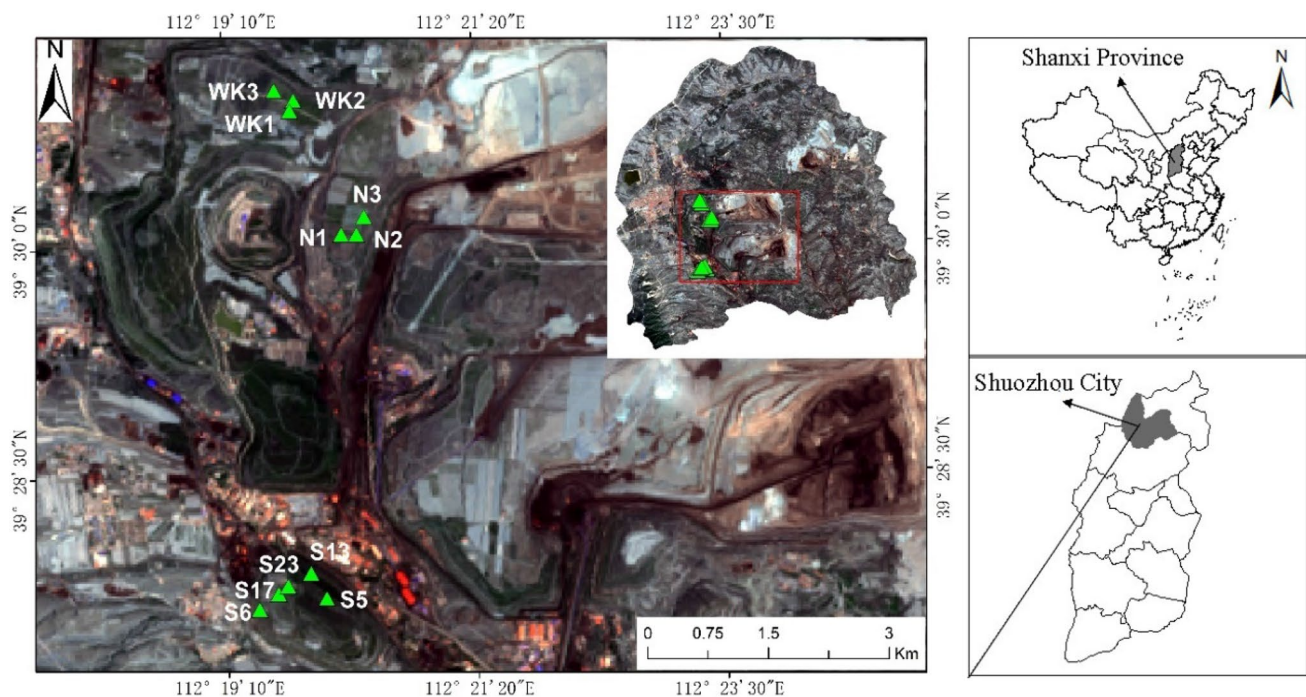


**Fig. 1** Antaibao open-pit mine, China coal mine

concentrated in July, August, and September. The amount of evaporation is approximately five times that of annual precipitation, which makes the soil in the mining area dry, water-poor, and prone to flood disasters and soil erosion. The soil is sandy and has a poor water retention capacity. This has limited the restoration of the ecosystem in the mining area and made the ecological environment fragile (Luo et al. 2021a, b; Xu et al. 2021). Reclamation began in 1990, and the vegetation allocation mode of "grass-shrub-arbor" was adopted (Xu et al. 2010; Guo et al. 2014) (Table 1).

### Data sources and testing

To comprehensively consider the climate and land cover in the study area, and to avoid the impact of concentrated rainfall on the test results when using GPR to detect the soil moisture content, our tests were conducted in May 2018 and May 2019 during the non-rainy season. On the west side of the mine, 35 points were identified; because of objective factors, the number of samples using the GPR for detection reached 25. In May 2019, we set up three sampling locations in the western dump, expanded western dump, and internal dump (Fig. 2). A total of nine samples were collected, and necessary field information was recorded in detail, such as altitude, terrain, slopes factors, slope directions, and vegetation types.

If the angle of the platform was between 0° and 2°, a quadrant with a size of 10 m × 10 m was set directly on the dump platform. On the dump slope, the width of the quadrat was set to 10 m, and the length of the quadrat was determined according to the slope. In the large 10 m × 10 m sample square, the area was randomly set to 1 m × 1 m. Plant residues and impurities were removed from the soil surface. Soil samples were collected using a cutting ring (Φ100) at 0–10, 10–20, 20–30, 30–40, 40–50, and 50–60 cm in each soil profile. The numbered ring cutter samples were immediately weighed, and their weights were recorded. After returning to the laboratory, each ring sample was placed into an oven at 105 °C and baked for 8 h until reaching a constant weight. RSBBD was calculated

**Table 1** Standard deviation of RSBBD

Samples	Geographical Coordinates	Information
S5	N:39° 27' 42" E:112° 20' 01"	Soil and rock profile
S6	N:39° 27' 38" E:112° 19' 26"	Pure soil profile
S13	N:39° 27' 52" E:112° 19' 53"	Soil and rock profile
S17	N:39° 27' 44" E:112° 19' 36"	Pure soil profile
S23	N:39° 27' 47" E:112° 19' 41"	Pure soil profile
WK1	N:39° 30' 58" E:112° 19' 47"	Pure soil profile
WK2	N:39° 30' 54" E:112° 19' 45"	Pure soil profile
WK3	N:39° 31' 02" E:112° 19' 37"	Pure soil profile
N1	N:39° 30' 05" E:112° 20' 11"	Pure soil profile
N2	N:39° 30' 05" E:112° 20' 19"	Pure soil profile
N3	N:39° 30' 12" E:112° 20' 23"	Pure soil profile



**Fig. 2** Typical sample profile

three times based on the international common method, the calculation formula of which is shown as follows:

$$\rho = \frac{M - m}{V}, \quad (1)$$

where  $\rho$  is RSBD,  $\text{g cm}^{-3}$ ;  $V$  is the ring knife volume,  $100 \text{ cm}^3$ ;  $m$  is the weight of the ring knife,  $\text{g}$ ; and  $M$  is the total weight of the ring knife and the dried soil,  $\text{g}$ .

### Processing of GPR detection images

GPR is a non-destructive detection technology that uses the reflection of electromagnetic waves to detect underground media (Bian et al. 2010; Chen et al. 2015; Chabukdhara and Singh 2016). GPR is mainly composed of the host computer, project antenna, and receiving antenna. When electromagnetic waves encounter an interface between two media, energy attenuation occurs; the round-trip durations of the electromagnetic waves, amplitudes, and waveforms reveal the corresponding media differences, and the target body morphology, spatial location, and structure are interpreted (Olhoeft 2000; Jonard et al. 2013; Luo et al. 2019a, b). After a section is dug, steel tubes with diameters of 3 cm, 4 cm, and 6 cm are drilled into sections at different depths into the GPR detection surface, and then, GPR is used for surface-based detection, which includes small sample detection and large sample detection ranges (Fig. 3). The speed is set to  $0.1 \text{ m ns}^{-1}$ , the permittivity is set to 9, and the GPR system is used to detect the  $10 \text{ m} \times 10 \text{ m}$  and  $1 \text{ m} \times 1 \text{ m}$  samples. In the detection process, the two methods of integral gain

and segmented gain are adopted for radar data processing. The overall gain is adjusted to 20 dB, and the optimal result is obtained by measuring the gain three times. The ground-penetrating radar is LTD-2600 with a frequency of 900 MHz, which was provided by the China Research Institute of Radio Propagation. The radar image processing software used to process the collected radar images was IDSP7.0.

According to the calibrated depth and propagation time of the steel tube, the propagation velocity of electromagnetic waves in different soil layers can be determined. Formula (2) is used to calculate the dielectric constant of different layers within a medium

$$\varepsilon = (c/v)^2, \quad (2)$$

where  $\varepsilon$  is the dielectric constant;  $c$  is the speed of light ( $3.00 \times 10^8 \text{ m s}^{-1}$ ); and  $v$  is the propagation speed of the electromagnetic wave signal through a medium.

## Results and analysis

### Profile characteristics of RSBD

RSBD in different dumps was collated and analyzed, and its average value and standard deviation were calculated (Table 2). In this paper, only RSBD data collected at depths of 0–10 cm and 10–20 cm were included in S5 and S13; therefore, Table 2 did not include S5 and S13. Within



Fig. 3 Calibration of profile depth in a targeted quadrant

**Table 2** Standard deviation of RSBD

Samples	S6	S17	S23	WK1	WK2	WK3	N1	N2	N3
Average	1.18	1.37	1.41	1.65	1.43	1.63	1.56	1.75	1.71
Standard deviation	0.05	0.08	0.14	0.10	0.08	0.03	0.06	0.13	0.10

the depth range of 0–60 cm, the average RSBD of most samples was greater than  $1.40 \text{ g cm}^{-3}$  (except for S6 and S17). Moreover, the average RSBD of S6 was the smallest ( $1.18 \text{ g cm}^{-3}$ ), while that of N2 ( $1.75 \text{ g cm}^{-3}$ ) was the highest, indicating that the maximum RSBD difference among these samples reached  $0.57 \text{ g cm}^{-3}$ . There were significant differences in the average value of RSBD among different dumps, especially between the southern dump (S6) and the internal dump (N2).

The standard deviation is used to represent the difference in RSBD at different depths. The standard deviation of S23 was 0.14, which was the largest among all samples, RSBD in 10–20 cm of S23 was relatively low and less than the average  $1.41 \text{ g cm}^{-3}$ , while RSBD in 30–60 cm was higher than the average value, especially when considering that RSBD in 40–50 cm was  $1.64 \text{ g cm}^{-3}$ . The standard deviation of WK3 was 0.03, which was the smallest value among all samples, there was no significant difference in RSBD at different depths for WK3. The standard deviation of the other samples approximately fluctuates around 0.10.

### Qualitative analysis of RSBD differences

Differences in RSBD within a certain range can be qualitatively analyzed according to the large-amplitude signals or color differences in the GPR images. When electromagnetic waves encounter two kinds of media with great dielectric difference, they will be reflected at the interface of the two media, and their energy will decay, which is shown as a large-amplitude signal in GPR images (Luo et al. 2019a, b). When encountering medium-sized divergence from RSBD at different depths, the electrical conductivity and dielectric constant will vary. When there is sufficient electrical difference between adjacent mediums, electromagnetic wave reflection occurs; the greater the energy attenuation and larger the electric property differences between adjacent media are, the greater the reflection and the faster the energy attenuation will be, driving the performance of GPR images for greater amplitude signals or color differences (Olhoeft 2000; Luo et al. 2019a, b). It provides a theoretical basis for the qualitative analysis of RSBD differences based on GPR images. IDSP7.0 was used to process GPR images (Fig. 4). Large amplitude signals in the GPR images were expressed.

### Retrieval of RSBD

Steel tubes with the diameters of 3 cm, 4 cm, and 6 cm were used to measure the soil dielectric constant. Based on the original amplitude data of the GPR images, the travel time of electromagnetic wave propagation was extracted (Fig. 5).

The varied soil volume moisture contents greatly impacted the dielectric constant, and samples in which the top layer soil volume moisture content was higher than 25% were removed, to prevent these data from influencing the final results. According to the soil volume moisture content at different depths, through many experiments that chose different ranges of soil moisture content, layers with soil volume moisture contents between 15 and 25% were chosen. Twenty-seven groups of RSBD values (Table 3) were calculated by the Formula (2). The dielectric constant of different soil media, the measured data of RSBD, and the GPR permittivity of the corresponding layers were fitted, and a fitted relationship model was established. Before the fitting analysis, it was assumed that RSBD at the sample's depth was close to RSBD at the calibration depth. The fitting analysis results are shown in Fig. 6. According to the fitting relationship, there is a negative correlation between RSBD of different dumps and the dielectric constant, producing an  $R^2$  of 0.52 ( $sig < 0.001$ ); thus, the fitting effect was considered reliable. Twenty-seven dielectric constants were substituted into the fitting relationship model in Fig. 6 to carry out RSBD inversion, and the inversion results were calculated (Table 4). Through comparison, it was found that RSBD obtained by model inversion was slightly higher than the measured RSBD, and the maximum absolute value of RSBD difference measured by the two methods was  $0.29 \text{ g cm}^{-3}$ , and the minimum was  $0.01 \text{ g cm}^{-3}$ .

## Discussion

### GPR images' recognition of RSBD

According to the corresponding sample images, large-amplitude signals increase, and RSBD decreases. Based on the calibrated depth of the steel tube and its corresponding travel time, the corresponding time ranges of different depths in the GPR images can be roughly judged. For S17, the depth of 0–20 cm corresponds to approximately 0–3.88 ns in the GPR images. At 10–30 cm, there are many large-amplitude signals in the GPR images, indicating a large difference in

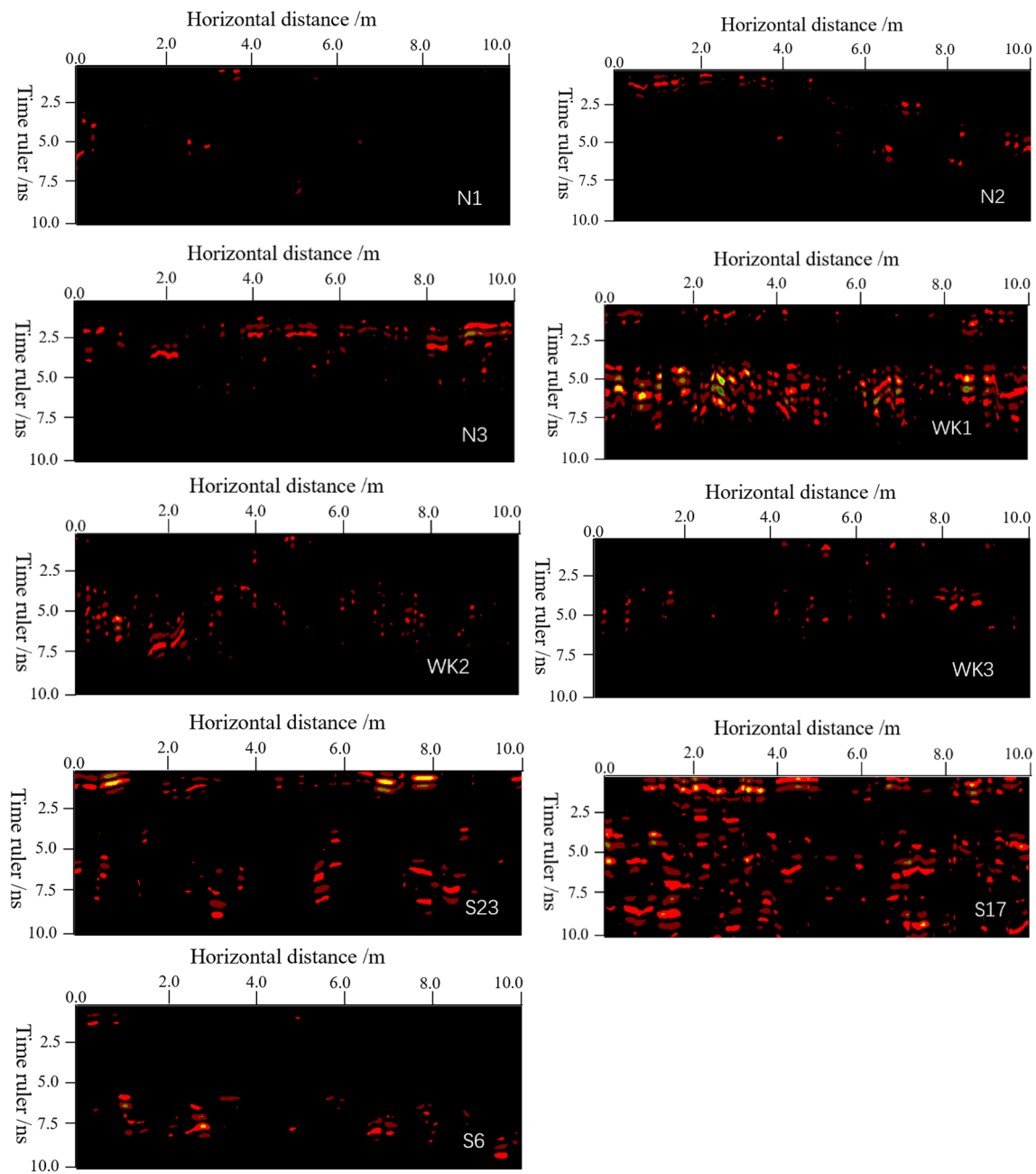


**Fig. 4** Difference in RSBD based on GPR images. The red parts in the figures represent large-amplitude signals

vertical impedance contrast of RSBD between layers within this range. For N2, most of the large-amplitude signals are plotted at the top of the images, and the large-amplitude signal is lower in the smaller radar images. The 0–20 cm depth corresponds to approximately 0–2.66 ns in the GPR images. The GPR images have many large-amplitude signals that fall within the scope of the larger RSBD differences, and the variations in RSBD at different depths are significant. For S23, the depth interval of 30–50 cm corresponds to 5.68–9.25 ns in the GPR images. At depths of 30–50 cm, there are many

large-amplitude signals in the GPR images, because soil volume moisture content is 15.87% at 30–40 cm and 21.97% at 40–50 cm, there is a large difference in vertical impedance contrast of reconstructed soil volume moisture content between layers within this range. For WK1, the 0–20 cm depth interval corresponds to 0–4.58 ns in the GPR images. There are many large-amplitude signals in this range, because there is obvious dry–wet stratification at a depth of 10 cm in this sample, and the moisture content exerts a great influence on the GPR images. For N3, the 0–15 cm

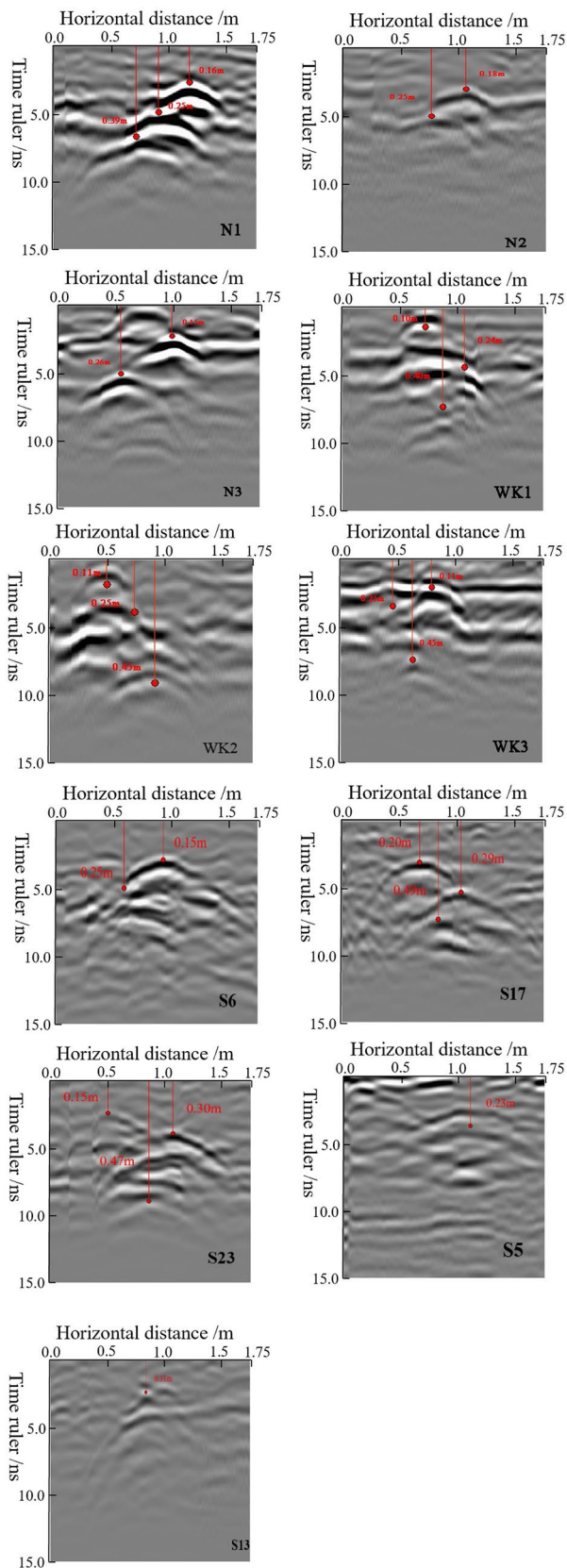


**Fig. 5** Depth calibration based on the GPR images. The red parts in the figures represent the calibration depth of steels

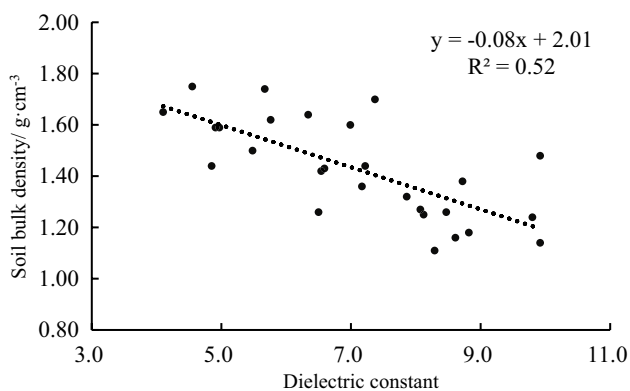
depth interval corresponds to 0–2.23 ns in the GPR images; the large-amplitude signal is lower and the soil porosity is larger in the images below 2.23 ns, which have more large-amplitude signals. The phenomenon can be explained by that there is a large amount of clay at 10–35 cm, with obvious material quality differences between the lower levels, which exerts a great influence on the GPR images. For WK2, the depth interval of 20–40 cm corresponds to 1.76–6.92 ns in the GPR images. There are many large-amplitude signals within this range, which corresponds to the great variability in the measured RSBD within this range. For N1, WK3 and S6, there are few large-amplitude signals in the GPR images, and the signal distribution is more uniform, indicating that there is lower contrast in RSBD of this sample in depth layer boundaries. A relationship was presented between the large-amplitude signal of the GPR images and RSBD differences in depth layer boundaries. When there are more large-amplitude signals, the corresponding RSBD difference is small. This principle is applicable in most cases, but if there is a large difference in the soil moisture content or soil texture, the conclusion obtained using this principle will experience certain deviations, which need to be adjusted according to the actual situation.

### Fitting effect of RSBD and dielectric constants

Among the factors that affect permittivity, the soil volume moisture content has a greater impact (Plati and Loizos 2013; Luo et al. 2019a, b). This article sampled data during the non-rainy season, and RSBD was more important to affect the dielectric constant. Before the fitting analysis, the soil volume moisture content was excluded, because it was too large to avoid the impact of large soil volume moisture contents on the test results. The fitting results show that there is a negative correlation between RSBD and the dielectric constant when the soil volume moisture content is between 15 and 25%, and the fitting function is  $y = -0.08x + 2.01$ . This paper chooses a soil moisture content between 15 and 25%, because when the soil volume moisture content is too large, the effect of soil moisture on the dielectric constant will mask the influence of RSBD. However, through field tests, it was found that many times when the soil volume moisture content is between 15 and 25%, the effects of RSBD on the dielectric constant are still obvious and will not be concealed by the soil volume moisture content. According to the fitting results, when the soil volume moisture content is between 15 and 25%, where  $R^2 = 0.52$  ( $sig < 0.001$ ), there is a negative correlation between RSBD and the corresponding dielectric constant when the soil volume moisture content is between 15 and 25% for different dumps in the North Shanxi open-pit mining area, which is roughly the same as the results obtained by relevant research using laboratory designs and experiments (Yamileth et al.

**Table 3** Detection parameter values of GPR at different depths

Samples	Calibration depth/cm	Propagation time/ns	Propagation velocity/(m ns <sup>-1</sup> )	Dielectric constant	Volume moisture content (%)
S5	0–23	4.37	0.11	8.12	23.35
S6	0–15	2.97	0.10	8.82	17.24
	15–25	1.92	0.10	8.29	15.14
	0–25	4.89	0.10	8.61	16.70
S13	0–11	2.31	0.10	9.92	23.59
S17	0–20	3.88	0.10	8.47	18.01
	20–29	1.54	0.12	6.59	21.43
	0–29	5.42	0.11	7.86	19.15
	29–49	3.41	0.12	6.54	21.27
S23	0–49	8.75	0.11	7.17	19.99
	0–15	3.13	0.10	9.8	17.45
	15–30	2.55	0.12	6.5	16.30
	0–30	5.68	0.11	8.07	17.10
	30–47	3.57	0.10	9.92	18.92
WK1	0–47	9.25	0.10	8.72	17.83
	0–10	2.58	0.09	10.4	13.00
	10–24	1.99	0.14	4.55	18.36
	24–40	2.54	0.13	5.67	18.42
WK2	0–40	7.24	0.11	7.37	16.64
	0–11	1.76	0.13	5.76	12.67
	11–29	2.81	0.13	5.48	17.52
WK3	29–45	2.35	0.14	4.85	15.44
	0–45	8.06	0.11	7.22	15.72
	0–11	2.15	0.1	8.6	10.69
	11–25	2.35	0.12	6.34	20.29
N1	25–45	2.7	0.15	4.1	19.99
	0–45	7.2	0.13	5.76	17.95
	0–16	2.82	0.11	6.99	18.46
N2	0–18	2.66	0.14	4.91	21.82
N3	0–15	2.23	0.13	4.97	15.29

**Fig. 6** The fitting relationship between RSD and dielectric constant

2019; Ersahin and Brohi 2006). However, the soil dielectric constant is affected by multiple factors, including soil texture, soil organic matter content, soil volume moisture content, soil porosity, etc. Although soil texture and soil organic matter content are secondary influencing factors, they still exert a small influence on the soil dielectric constant (Luo et al. 2019a, b; Wang et al. 2016a, b). In this paper, a certain segment of the samples ran through sandy soil mixed with clay; the soil texture had an effect on the dielectric constant, which increased the error of the fitted curve and the fitting function. Therefore, different soil types should be considered in future research when other soil textures and organic matter contents can be collected. The influence of soil organic matter should be considered to improve the accuracy of the fitting function.



**Table 4** Comparison of sample measurement and model inversion of RSBD at different depths of each profile

Sampling points	Calibration depth/cm	RSBD/g cm <sup>-3</sup>			
		Sample measurement	Model inversion	Measurement inversion	
S5	0–23	1.18	1.30	–0.12	
S6	0–15	1.11	1.34	–0.23	
	15–25	1.16	1.31	–0.15	
	0–25	1.26	1.32	–0.06	
S13	0–11	1.43	1.48	–0.05	
S17	0–20	1.32	1.37	–0.05	
	20–29	1.42	1.48	–0.06	
	0–29	1.36	1.43	–0.07	
	29–49	1.24	1.21	0.03	
	0–49	1.26	1.49	–0.23	
	S23	0–15	1.27	1.36	–0.09
		15–30	1.48	1.20	0.28
0–30		1.38	1.30	0.08	
30–47		1.75	1.65	0.10	
0–47		1.74	1.55	0.19	
WK1	10–24	1.70	1.41	0.29	
	24–40	1.50	1.57	–0.07	
	0–40	1.44	1.62	–0.18	
WK2	11–29	1.44	1.43	0.01	
	29–45	1.64	1.50	0.14	
	0–45	1.65	1.68	–0.03	
WK3	11–25	1.62	1.55	0.07	
	25–45	1.60	1.45	0.15	
	0–45	1.59	1.62	–0.03	
N1	0–16	1.59	1.61	–0.02	
N2	0–18	1.25	1.35	–0.10	
N3	0–15	1.14	1.20	–0.06	

### Feasibility of GPR in detecting RSBD

The earliest application of GPR was in the field of engineering quality, which mainly focused on non-destructive quality testing. After decades of development, using GPR to detect the soil physical properties have been widely used and recognized (Wang et al. 2017; Wang 2011; Wang et al. 2016a, b). Similar to the application principle utilized in the field of engineering quality inspection, qualitative and quantitative analyses of RSBD based on GPR have been carried out locally and abroad. Some researchers have used electromagnetic wave velocity and amplitude analyses to invert RSBD, and believed that RSBD is inversely proportional to the electromagnetic wave velocity and negatively correlated with the maximum amplitude of electromagnetic waves (Wang et al. 2016a, b). According to the principle of utilizing a single variable, some scholars have established

mathematical models of RSBD and dielectric constants through laboratory design experiments. It was found that under the condition of unsaturated soil, RSBD and the corresponding dielectric constant showed a negative correlation in some cases, but the specific relationships and mechanisms have not been explored (Wang et al. 2016a, b). In conclusion, in the unsaturated soil state, the relative variation in RSBD can be qualitatively analyzed on the GPR signal map using the dielectric conductivity parameter of a medium, and the real value of RSBD can be quantitatively estimated using the dielectric constant of the medium-RSBD model. Due to the numerous interference factors involved in field testing, most research has stayed in the laboratory verification stage without actual applications in mining areas, resulting in the complex reconstruction of soils in mining area reclamation; therefore, GPR technology rarely achieves the expected effect. According to the experiment results in this paper, it is concluded that large-amplitude signals distributions in radar images can be employed to detect the variations of RSBD at different depths. Such analyses would show a greater large-amplitude signal within a given depth range; the greater RSBD differences and large-amplitude signals are, the greater the variability of RSBD will be.

In soil volume moisture contents between 15 and 25%, GPR technology can quantitatively estimate RSBD using the radar electromagnetic wave propagation. It can be concluded that when considering depth within the scope of propagation velocities, the transmission speed in empirical formulas can be used to obtain the corresponding dielectric constant. According to the relevant mathematical model setup in this article, you can test within the scope of RSBD estimates, within a certain range of error, the approximate estimates can be obtained instead of the measured values. This methodology can be applied to other regions with similar climate characteristics of the study area and used for other open-pit mine land reclamation projects aiming to carry out quality inspection work. This greatly improves the feasibility of the practical application and popularization of GPR; however, when considering the process of popularization and use, appropriate adjustments should be made according to the actual situation of the measured area. For the areas with highly variable soil textures and excessive soil moisture contents or even saturated conditions, this method has limitations, and the estimated value obtained by this method may report a large deviation from the actual measured value. Therefore, this theory does not apply to the above two areas.

### Conclusion

1. RSBD showed obvious variations at different depths of the same soil profile and in different dumps of the mining area.

2. The differences in RSBD can be qualitatively analyzed according to the distribution of the large-amplitude electromagnetic wave signal in GPR images. When there are fewer large-amplitude electromagnetic wave signals, the vertical impedance contrast of density between layers is small, and the difference of RSBD is small too. The difference in RSBD can be estimated roughly according to the above theory.
3. When the soil volume moisture content is between 15 and 25%, the relationship between the dielectric constant and RSBD can be described by a reliable fitting function ( $y = -0.08x + 2.01$ ,  $R^2 = 0.52$ ,  $sig < 0.001$ ). When the soil volumetric moisture content is between 15 and 25%, RSBD can be retrieved from the soil dielectric constant based on the negative linear relationship. This study validated the applicability of GPR in detecting RSBD of reclaimed lands, which provided some inspiration for the land reclamation in the open-pit mining regions of similar ecosystems.

**Acknowledgements** This study was funded by the National Natural Science Foundation of China (41701607, U1810107) and the Basic Scientific Research Foundation for Excellent Supervisors, Ministry of Education, P. R. China (2-9-2018-025, 2-9-2019-307).

## Declarations

**Conflict of interest** We have declared that we do not have any commercial or associative interest that represents a conflict of interest in connection with the work submitted.

## References

- Abu-Hamdeh NH (2003) Compaction and subsoiling effects on corn growth and soil bulk density. *Soil Sci Soc Am J* 67:1213–1219
- Anchuela OP, Luzon A, Perez A et al (2016) GPR evaluation of the internal structure of fluvial tufa deposits (Dévanos-Añavieja system, NE Spain): an approach to different scales of heterogeneity. *Geophys J Int* 206(1):557–573
- Andrea B (2010) Water content evaluation in unsaturated soil using GPR signal analysis in the frequency domain. *J Appl Geophys* 71(1):26–35
- Berton F, Guedes CC, Vesely FF et al (2019) Quaternary coastal plains as reservoir analogs: wave-dominated sand-body heterogeneity from outcrop and ground-penetrating radar, central Santos Basin, southeast Brazil. *Sed Geol* 379(1):97–113
- Bian ZF (2005) Research on the reclamation and ecological reconstruction in coal mining area in China. *Resour Ind* 02:18–24
- Bian Z, Inyang HI, Daniels JL et al (2010) Environmental issues from coal mining and their solutions. *Min Sci Technol (China)* 20(2):215–223
- Brahim N, Bernoux M, Gallali T (2012) Pedotransfer functions to estimate soil bulk density for northern Africa: Tunisia case. *Arid Environ* 81:77–83
- Bunker SG (1996) Raw material and the global economy: oversights and distortions in industrial ecology. *Soc Nat Resour* 9:419–429
- Buttel FH (2002) Environmental sociology and the sociology of natural resources: institutional histories and intellectual legacies. *Soc Nat Resour* 15:205–211
- Cao YG, Bai ZK, Zhang GJ et al (2013) Soil quality of surface reclaimed farmland in large open-cast mining area of Shanxi province. *J Agro-Environ Sci* 32(12):2422–2428
- Cao YG, Wang JM, Bai ZK et al (2015) Differentiation and mechanisms on physical properties of reconstructed soils on open-cast mine dump of loess area. *Environ Earth Sci* 74(8):6367–6380
- Cao YG, Bai ZK, Sun Q et al (2017) Rural settlement changes in compound land use areas: characteristics and reasons of changes in a mixed mining-rural-settlement area in Shanxi province, China. *Habitat Int* 61:9–21
- Cao YG, Dallimer M, Stringer LC et al (2018) Land expropriation compensation among multiple stakeholders in a mining area: explaining “skeleton house” compensation. *Land Use Policy* 74:97–110
- Chabukdhara M, Singh OP (2016) Coal mining in northeast India: an overview of environmental issues and treatment approaches. *Int J Coal Sci Technol* 3(2):87–96
- Chen J, Ge SC, Zhao YH et al (2015) Wavelet processing and interpretation of radar detection image of seawall hidden danger. *Chin J Undergr Space Eng* 11(S1):337–341
- Chen XY, Wang F, Yan JP et al (2016) Effects of soil thickness on day and night changes of reclaimed soil respiration in mining area. *J China Univ Min Technol* 45(1):163–169
- Ersahin S, Brohi AR (2006) Spatial variation of soil water content in topsoil and subsoil of a Typic Ustifluent. *Agric Water Manag* 83(1/2):79–86
- Guo LL, Wang JM, Zhang M et al (2014) Effects comparison of different reclamation modes in grassland opencast coalmine area. *Metal Mine* 6:150–155
- Han XL, Liu JT, Zhang J et al (2016) Identifying soil structure along headwater hillslopes using GPR based technique. *J Mt Sci* 13(3):405–415
- Jonard F, Mahmoudzadeh M, Roisin C et al (2013) Characterization of tillage effects on the spatial variation of soil properties using ground-penetrating radar and electromagnetic induction. *Geoderma* 207–208:310–322
- Kitula AGN (2006) The environmental and socio-economic impacts of mining on local livelihoods in Tanzania: a case study of Geita District. *J Clean Prod* 14(3–4):405–414
- Li RX, Lin CH, Gao HW (2001) Variance analysis of soil compaction caused by agricultural machinery. *Agric Mech Res* 3:84–87
- Li RX, Lin CH, Gao HW et al (2002) Research on soil compaction by small wheeled tractor. *Trans Chin Soc Agric Eng* 1:126–129
- Luo GB, Cao YG, Bai ZK et al (2019a) Soil bulk density difference, ground penetrating radar feature identification, and simulation for a reclaimed soil profile in the dumping site of an open pit mine. *J Agric Resour Environ* 36(4):441–452
- Luo GB, Cao YG, Kuang XY et al (2019b) Research progress of detection of typical soil physical properties based on ground penetrating radar. *Jiangsu Agric Sci* 47(14):40–44
- Luo GB, Cao YG, Xu HX et al (2021a) Detection of soil physical properties of reclaimed land in open-pit mining area: feasibility of application of ground penetrating radar. *Environ Monit Assess* 193:392
- Luo GB, Cao YG, Xu HX et al (2021b) Research on typical soil physical properties in a mining area: feasibility of three-dimensional ground penetrating radar detection. *Environ Earth Sci* 80:92
- Ma R, Han WB, Bai ZK (2006) Research of ravaged indexes of water and soil loss of dumping site of large opencast coal mine in loess area-example for the south dumping site of Antaibao open-cast coal mine. *Energy Environ Prot* 2:50–53
- Mondal S, Maiti KK, Chakravarty D et al (2016) Detecting risk buffer zone in open-cast mining areas: a case study of Sonepur-Bajari, West Bengal, India. *Spat Inf Res* 24(6):649–658

- Olhoeft GR (2000) Maximizing the information return from ground penetrating radar. *J Appl Geophys* 43:175–187
- Osunbitan JA, Oyedele DJ, Adekalu KO (2005) Tillage effects on bulk density, hydraulic conductivity and strength of a loamy sand soil in southwestern Nigeria. *Soil till Res* 82(1):57–64
- Pan J, Bai ZK, Cao YG et al (2017) Influence of soil physical properties and vegetation coverage at different slope aspects in a reclaimed dump. *Environ Sci Pollut Res* 24(30):23953–23965
- Plati C, Loizos A (2013) Estimation of in-situ density and moisture content in HMA pavements based on GPR trace reflection amplitude using different frequencies. *J Appl Geophys* 97:3–10
- Sun Q, Bai ZK, Cao YG et al (2015) Ecological risk assessment of land destruction in large open-pit mine. *Trans Chin Soc Agric Eng* 31(17):278–288
- Wang W (2011) Research on GPR quantitative detection technology for high-grade highway pavement subgrade. Ocean University of China, Qingdao
- Wang ZC, Wu W (2010) Geological radar technology for nondestructive testing of tunnel quality. *Railw Technol Innov* 3:78–80
- Wang L, Zhang HS (2013) The research progress of land reclamation in mining area in domestic and abroad. *Res Soil Water Conserv* 20(1):294–300
- Wang JM, Guo LL, Bai ZK et al (2016a) Effects of land reclamation time on soil pore number and porosity based on computed tomography (CT) images in opencast coal mine dump. *Trans Chin Soc Agric Eng* 32(12):229–236
- Wang P, Hu Z, Zhao Y et al (2016b) Experimental study of soil compaction effects on GPR signals. *J Appl Geophys* 126:128–137
- Wang BB, Sun B, Tian G et al (2017) Analysis of sea ice thickness and surface morphological characteristics of Arctic summer using three-dimensional GPR. *Geophys Geochem Explor* 31(3):189–192
- Wu YB, Cui F, Wang L et al (2014) Detection of soil moisture content by transmissive ground penetrating radar. *Trans Chin Soc Agric Eng* 30(17):125–131
- Xu JW, Li JC, Bai ZK et al (2010) Effect of reclamation land soil to plant diversity in Antaibao opencast coal mine loess zone—a case of discharged soil field in Antaibao opencast coal mine. *J Shanxi Agric Sci* 38(4):48–51
- Xu HX, Cao YG, Luo GB et al (2021) Differences of reconstructed soil bulk density in open pit mine of northern Shanxi province: based on feature identification and inversion of ground penetrating radar. *J Ecol Rural Environ* 37(1):127–135
- Yamileth DH, Elena V, Jesús C (2019) Evaluation of reclamation success in an open-pit coal mine using integrated soil physical, chemical and biological quality indicators. *Ecol Ind* 103:182–193

**Publisher's Note** Springer Nature remains neutral with regard to jurisdictional claims in published maps and institutional affiliations.